

A conceptual design and FE analysis of a piezoceramic actuated dispensing system for microdrops generation in microarray applications

Pinhas Ben-Tzvi ^a, Ridha Ben Mrad ^{b,*}, Andrew A. Goldenberg ^a

^a Robotics and Automation Laboratory, Department of Mechanical and Industrial Engineering, University of Toronto, 5 King's College Road, Toronto, Ont., Canada M5S 3G8

^b Mechatronics and Microsystems Design Laboratory, Department of Mechanical and Industrial Engineering, University of Toronto, 5 King's College Road, Toronto, Ont., Canada M5S 3G8

Received 31 October 2005; accepted 4 August 2006

Abstract

In recent years, both the diagnostic and pharmaceutical industries have begun to seek improved methods of reagent dispensing that would enable them to reduce the amount of reagent used, improve the accuracy and repeatability of the quantities dispensed, and generally expedite the processing of assays and microarrays. This paper presents a design of a dispensing system for microdrops generation operated in a drop-on-demand mode using a non-contact liquid transfer method. Unlike existing methods for droplets generation, which operate in an open-loop, this system operates in a closed-loop manner. Therefore, the system can potentially generate droplets with very high accuracy up to several picoliters in order to generate very high-density microarrays. Detailed finite element analysis is used to optimize the design, assess the performance of the system, and define suitable operating parameters.

© 2006 Elsevier Ltd. All rights reserved.

Keywords: Dispensing system; Droplet generator; Microarrays; Piezoceramics; CFD

1. Introduction

There has been extensive work done on the development of micro-droplet generators since the ideas by Dr. Sweet of Stanford University in the early 1960's using piezo actuation, as well as work done at Hewlett-Packard and Cannon Corporation [1] in the late 1970's using thermal-bubble actuation. Sweet demonstrated that by applying a pressure wave pattern to an orifice, the liquid stream could be broken into droplets of uniform size and spacing [2]. Recently, with emerging applications in biomedicine, fuel injection, pharmaceuticals, electronic fabrication, and many others, micro-droplet generators are getting even more research interest. Thus, many new operation principles, designs, fabrication processes, and materials related to micro-droplet

generation were explored and developed during the last decade.

Droplet generators usually employ mechanical actuation to generate a high pressure to overcome the liquid surface tension and the viscous force for droplet ejection. Depending on the droplet size, the applied pressure is usually higher than several atmospheres. The operation principles, structure/process designs, and materials play key roles in the performance of droplet generators.

Applications of micro-droplet generators, in addition to the well known application of ink-jet printing include drug screening/delivery/dosage, direct writing, fuel injection, solid free form, solar cell fabrication, packaging, micro optical components, particle sorting, micro dosage, plasma spraying, micro propulsion, integrated circuit cooling, and chemical deposition. In many applications, a reliable and low-cost micro injector array is desired. In addition, the micro injector array also needs to supply high quality micro-droplets (e.g., very small droplet volume deviation,

* Corresponding author. Tel.: +1 416 946 3597; fax: +1 416 978 7753.
E-mail address: rbenmrاد@mie.utoronto.ca (R. Ben Mrad).

and droplet ejection without satellite droplets), and work at high frequency.

In recent years, both the diagnostic and pharmaceutical industries have begun to seek improved methods of reagent dispensing that would enable them to reduce the amount of reagent used and improve the accuracy and repeatability of the quantities dispensed. Accuracy and precision in the amount of fluid dispensed is important both from the standpoint of causing a desired chemical reaction and minimizing the amount of material used.

The forces driving the search for improved dispensing technologies include the need to increase the amount of diagnostic information that can be derived from a patient sample, and a generalized market pressure to reduce the cost of assays. Characteristics of a successful technology include the ability to handle a wide range of solvents and solutes, to dispense reagents in drop volumes in the range of picoliters, to introduce a great deal of functionality and control to the dispensing process, to execute various dispensing operations in an automatic mode with minimum manual handling, and to increase throughput by using non-contact dispensing methods.

In this paper, a brief overview of dispensing technology being used for microarraying is presented and a novel design of a high accuracy, high throughput and wide operating range droplet generator is then presented. The droplet generator is operated in closed-loop. A detailed finite element based analysis of the dispenser is pursued in order to appropriately select the various physical parameters of the droplet generator, to predict performance and to select appropriate operating parameters.

2. Categorization of droplet generators and their application in microarray spotting

Droplet generators can be categorized based on the following two main categories: dispensing modes of operation and liquid transfer modes.

2.1. Dispensing modes of operation

A droplet generator can operate in any one of the following three distinct modes [3–5]: drop-on-demand, continuous, or burst mode of operation. The drop-on-demand mode operation is sometimes referred to as *Non-Pressure Generator*. This mode [1,6,7] was developed from ink-jet computer printer technology. By means of piezoelectric materials (piezoelectric actuation) or thin film resistor (thermal-bubble actuation), a pressure wave is produced in a capillary system filled with fluid. The fluid is maintained at ambient pressure and the actuating element is used to create a drop only when needed. The transducer creates a volumetric change in the fluid that creates pressure waves. The pressure waves that travel to the orifice are converted into fluid velocity, which results in a drop being ejected from the orifice [8,9]. Drop-on-demand mode droplet generator systems produce droplets that are

approximately equal in diameter to the orifice diameter of the droplet generator [10]. Non-pressure generators can produce, as required, single droplets, sequences and droplet chains in the kHz range. Sample amounts can be reduced to less than few picoliters, which results in delivering an extremely precise dispensing of the liquid. For the production of droplets with a diameter of less than 50 μm , the drop-on-demand system usually offers the most advantages.

The continuous dispensing mode of operation is sometimes referred to as *overpressure generator*. In a continuous mode droplet generator, pressurized fluid is forced through an orifice, typically 50–80 μm in diameter, to form a liquid jet. Surface tension acts to amplify even minute variations in the jet diameter, causing the jet to break up into droplets. This behavior is referred to as Rayleigh break-up [11]. If a single frequency disturbance, in an appropriate frequency range, is applied to the jet, then this disturbance will be amplified and droplets of extremely repeatable size and velocity are generated at the applied disturbance frequency. The disturbance is usually generated by an electromechanical device (e.g., a piezoelectric transducer), which creates pressure oscillations in the fluid. Generators in the overpressure range are continually producing droplets at high frequencies. They, therefore, use relatively large test amounts.

Generator operation in the burst mode is basically the same as that described for droplet-on-demand operation. However, the addition of a second pulse generator in the electrical control element allows modification of the actuating element drive voltage pulse train for production of a burst or packet of individual droplets [5].

2.2. Liquid transfer modes

The technologies for transferring liquid onto a substrate fall into two distinct categories: Non-contact and contact dispensing. Contact dispensing involves direct contact between the dispensing mechanism and the solid support. Contact printing devices include solid pins, capillary tubes, tweezers, split pins and micro-spotting pins or “ink stamps”, all of which deliver sample spots onto the solid surface. In surface contact dispensing, the pin tools are dipped into the fluid, resulting in the transfer of a small volume of fluid onto the tip of the pins. Touching the pins or pin samples onto the surface leaves a spot, the diameter of which is determined by the surface energies of the pin, fluid, and substrate.

Non-contact dispensing involves the ejection of drops from a dispenser onto the surface. The most common type of non-contact dispensing uses ink-jet printing technologies, which are essentially modifications of devices used for printing ink onto paper. As a non-contact dispensing process, the volumetric accuracy of dispensing is not affected by how the fluid wets a substrate, as is the case when pin transfer systems touch the substrate during the dispensing event. In addition, the fluid source cannot be contaminated by the substrate, as is the potential during

pin transfer touching. Finally, the ability to free fly the droplets of fluid over a millimeter or more allows fluids to be dispensed into wells or other substrate features. The non-contact dispenser's versatility is demonstrated by the ability to vary dot size rapidly and be integrated into most platforms easily. Changing the number of shots in one location can quickly change the dot size. If a larger dot is required then the dispenser can shoot additional dots on top of each other to increase the dot size. The fast cycle rate allows the dispenser to shoot multiple dots without greatly reducing the platform throughput.

2.3. Droplet generators in DNA microarray spotting

DNA Microarray technology enables the simultaneous analysis of thousands of sequences of DNA for genomic research and diagnostics applications. Making a Microarray by printing involves delivering a small volume of DNA sample onto the solid surface. The volume delivered is typically in the nL (10^{-9} L) or pL (10^{-12} L) range. The technologies for spotting DNA material onto a substrate fall into two distinct categories: non-contact and contact dispensing modes (see Section 2.2). Two major types of non-contact dispensers, piezoelectric and syringe solenoid [12] are currently being used to print DNA microarrays. Contact spotting is a more traditional method, which has limitations in speed and consistency. Future innovations in spotting technologies appear to be more focused on non-contact methods, such as piezoelectric based dispensers. Commercial developments on piezoelectric based dispensers have been led by Packard Instrument Company [13] and Incyte Pharmaceuticals [14]. Several good reviews are available on technologies and instrumentation for printing DNA microarrays [12,15].

2.4. Issues related to existing dispensing technologies and required specifications

The issues that lead to the need for a new dispensing paradigm and the problems related to existing dispensing technologies are briefly listed below.

1. There is no ability to detect, verify and control the dispensed droplet's volume in real-time in order to generate reproducible droplet size, which is essential in the fabrication of microarrays.
2. The range of liquid volumes that can be dispensed through the dispenser is limited and depends on the actuating element.
3. Extra equipment is required in order to aspirate liquids in addition to dispense liquids (usually a syringe pump and tubings are needed when liquids need to be loaded into the dispensing system).
4. There is no ability to detect and signal an improper operation of the device in real-time such as: misfiring (no droplet ejection has occurred), clogging of the nozzle, empty capillary and etc.

5. Lack of ability to recover from dispensing problems in real-time.

3. Design of the dispensing system for droplets generation

This section presents a design paradigm of a dispensing system for microdrops generation that operates in a closed-loop manner. The closed-loop approach overcomes various problems of existing systems and adds a great deal of functionality to the dispensing process, thereby optimizing stability and reproducibility of droplets generation.

A design describing the dispensing system is shown in Fig. 1 and includes: a piston in a glass capillary operated by an electrically controlled piezo-stack (N_1) and a stepper motor connected through a lead-screw; a second piezo-element (N_2) used as a pressure sensor (a detailed review on piezoelectric materials including applications and theory can be found in [16,17]); and an incremental encoder connected to the motor's shaft. This dispensing system is potentially capable of rapidly and accurately dispensing droplets in the range of picoliters, as will be shown in Section 4. The dispensing system is operated in a drop-on-demand mode of operation and in a non-contact liquid transfer method. This system can be mounted as a single

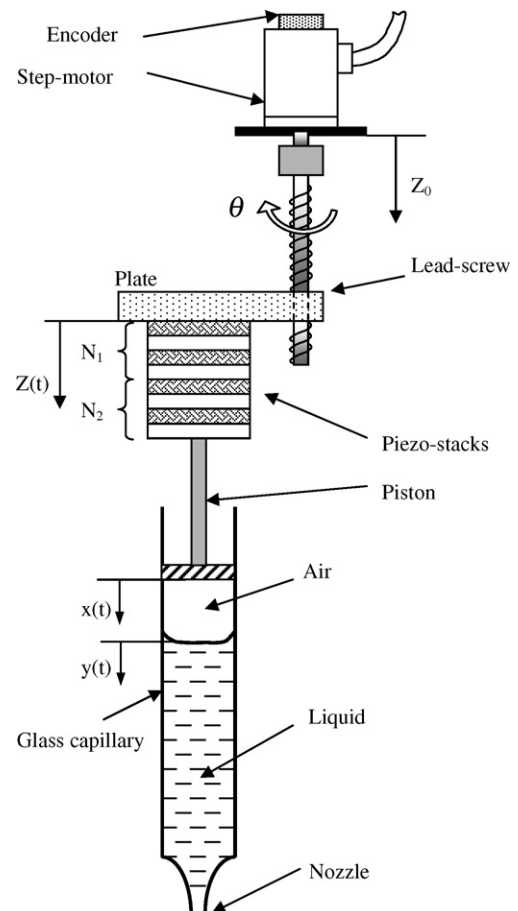


Fig. 1. Schematic of a piezo-driven-piston dispensing system.

channel or as an array of dispensers onto a multi-axis robotic system, which is used to position the dispensers at specific required locations and to execute any desired liquid transfer protocol.

3.1. System loading and initialization protocol

To prime the dispenser with liquid, a control unit directs a 3-axis robotic system to position the dispenser above the appropriate well in the microwell plate and then move downwards until dipped into the liquid. The position of the piston relative to the glass capillary and an inertial reference frame (Z_0) are known a priori, considering the amount of the initial air volume required inside the system. As depicted in Fig. 1, the air gap is situated between the piston and the liquid that is to be aspirated from the microwell plate. Digitally encoded commands to the stepper motor cause the piston to move in an upward direction and thereby forcing discrete amounts of liquid into the capillary through the nozzle.

The amount of the aspirated liquid volume can be precisely measured by knowing the inner diameter of the glass capillary and the upward movement of the piston that is continuously known from the encoder's reading. As soon as the initialization process is complete, the initial air and liquid volumes are defined. If necessary, after the system is primed, the piston is slightly moved downward until a liquid meniscus appears at the nozzle exit in order to build an appropriate initial pressure in the liquid's column.

3.2. The dispensing process

The system includes a liquid that is to be dispensed separated by a known volume of air, which is confined by the piezo-piston as shown in Fig. 1. The air gap is used in order to measure small changes of pressure in the liquid, which can be correlated to the volume of the dispensed liquid through calibration. It is much easier to calibrate the system such that it measures pressure changes associated with the volume change of one species only (air in this case). This way, the amount of dispensed liquid can be measured in a straight forward manner regardless of the liquid's properties.

Each time a droplet is dispensed, the liquid will return to its prior position inside the capillary due to capillary forces, and the air gap's volume will increase according to the amount of the dispensed liquid. Consequently, the pressure in the liquid column will decrease. The continuous pressure drop is monitored in real-time by the piezo-element (N_2). The piston is actuated (relative to axis Z) by another piezo-stack (N_1). The piston actuation continuously alters the air volume, which induces pressure pulses that drive the liquid. The deformation of the second piezo-element (N_2) due to the pressure inside the system, results in a generation of an electrical current. The electrical signals generated by piezo-element (N_2), indicate the corresponding pressure variation inside the capillary.

Depending on the properties of the dispensed liquid, an optimal range of positive pressure for stable and reproducible generation of droplets is defined through calibrations and should be continuously maintained and verified during the dispensing process. Below a certain amount of pressure, which should be greater than or equal to the atmospheric (ambient) pressure, the generation of droplets would be impossible. Therefore, during operation, if the pressure drops below the threshold value, the stepper motor will be continuously commanded to advance the piston (relative to the inertial frame of reference Z_0) in order to compensate for the pressure drop. This way the dispensing system can operate continuously. The number of piston actuations possible between two consecutive piston advancements by the stepper motor may be one or more. In other words, if the pressure needs to be increased after each piston actuation, there will be an alternating operation between the piston displacement by the piezo-stack and the piston advancement by the stepper motor.

Another way to monitor the amount of liquid that is being dispensed in real-time, in addition to monitoring changes in the pressure inside the capillary, is by monitoring the cumulative movement of the piston. The encoder reading (θ) is linearly correlated to the cumulative movement of the piston by the following expression:

$$Z = k \cdot \theta \quad (1)$$

where k is the gear ratio of the lead-screw and Z is the absolute movement of the piston.

Digitally encoded commands will cause the stepper motor not only to aspirate discrete volumes of liquid into the dispenser, but also to wash the dispenser between liquid transfers, and to control the pressure in the system. The stepper motor can also be used alone without actuating the piston with piezo-stack (N_1), when higher volumes of liquid should be dispensed through the dispenser.

If it is needed to eject liquid volumes in the range between the resolutions permitted by actuating the piston by the stepper motor alone or by the piezo-stack (N_1) alone, the dispenser will be directed to eject multiple droplets (when operated by the piezo-stack (N_1) alone), each having a predetermined volume, on the same location. Varying the magnitude and duration of the electrical signal applied to the dispenser can vary droplet size. Other factors affecting droplet size include the size of the nozzle opening at the bottom of the dispenser and the properties of the liquid.

The signals received from the pressure sensor (piezo-element N_2) are converted from an analog form into a digital form by an A/D (analog to digital) converter. At various points during the dispensing process, a control unit receives signals from the pressure sensor, and sends command signals to the stepper motor to advance the piston in order to compensate for the pressure drop during the dispensing process. Also, the measured pressure signals are processed and analyzed in order to: verify and quantify droplet volumes, perform diagnostics on the state of the dispensing

system, and automatically perform calibration of the dispenser for any selected liquid. The pressure sensor can sense fluctuations in pressure associated with priming the device, aspirating liquid, dispensing droplets, and washing the device. The pressure sensor converts pressure into electrical signals, which are used in order to detect various possible operation modes and therefore to orchestrate executions of appropriate algorithms. For example, when the device is dispensing or being primed, the pressure sensor will send electrical signals, which will be analyzed by a control unit. The control unit will determine whether the signals indicate any problem within the system such as exceptional increase in pressure (can occur when dispensing) or exceptional drop in pressure due to partial or complete blockage of the dispenser (can occur when priming).

A control unit determines the magnitude and duration of the voltage pulses, and also the frequency at which the pulses are to be sent to the dispenser. Each voltage pulse causes an elongation of the piezo-stack (N_1), which in turn moves the piston. The movements of the piston produce pressure waves that propagate through the air volume to the liquid towards the nozzle where droplets of liquid are emitted at a high acceleration. The high acceleration of the liquid minimizes or eliminates problems caused by liquid's surface tension and viscosity, allowing extremely small droplets to be expelled from the nozzle. The magnitude of the pressure drop is a function of the size of the air gap and the volume of the liquid dispensed. With an air gap of known volume, the pressure change, as detected by the pressure sensor, can be related to the volume dispensed. This relationship can be found by calibration experiments. The best way to do this is to incorporate look-up tables that correlate values of air pressure and volume.

In some applications, once the dispensing process has been completed, it is required to wash the dispenser. In such case, the internal surface of the glass capillary and the external surface of the nozzle area that were exposed to the liquid should be washed. Actuation of the piezo-stack in resonance can facilitate washing of the dispenser. While the stepper motor moves the piston in a relatively fast motion in order to eject the cleaning liquid that was aspirated, the piezo-stack vibrates at its resonance frequency. This joint actuation process is expected to be very effective in removing any matter adhering to the dispenser. Additionally, actuation of the dispenser at its resonance frequency also can be used to prevent, minimize or alleviate clogging of the nozzle not only in the dispensing process but also during aspiration of liquids.

3.3. Specifications and advantages of the system

The proposed design offers advantages as follows:

1. The ability to implement a closed loop control procedure for defining the droplet's size for different liquids of different properties.

2. A much wider range of liquid volumes can be dispensed through the dispenser due to the existence of two displacing mechanisms – namely, piezo-stack (N_1) and the stepper motor.
3. The ability to aspirate liquids in addition to dispense liquids with no need of extra equipment (usually a syringe pump and tubings are needed when liquids need to be loaded into the dispenser).
4. The ability to detect and verify the dispensed droplet volume in a real-time mode by sensing the corresponding changes in pressure.
5. Senses pressure changes associated with clogging and misfiring (indication of improper operation – namely, no droplet ejection has occurred). Zero change in pressure between any two consecutive cycles indicates misfiring.
6. Signaling when the capillary is empty by sensing sudden pressure drop and/or by monitoring the piston's movement.
7. Ability to detect and recover from dispensing problems in real-time.
8. Verify that the liquid is maintained within a given range of positive pressure, with respect to the ambient atmospheric pressure, in order to accurately dispense reproducible uniform droplets.

3.4. Control methods implementation

The liquid responds to inputs generated by displacements of the piston, but it is crucial to understand that the liquid would not respond to inputs, although inputs may exist, if a certain pressure is not maintained. The pressure plays a very important role in providing a physical linkage between the input (piston displacement) to the output (liquid response). In other words, during the dispensing process, it may happen that the air volume reaches a value that results in a pressure drop in a manner such that the liquid would not respond to the piston's displacements. Therefore, it is proposed that the pressure should be maintained by an "external" closed loop control method (Fig. 2).

As shown in Fig. 2, the voltage signals generated by the piezo-element are amplified, filtered, sampled and acquired by the control unit. The control unit then performs the following procedures in real-time:

1. Calculates the pressure in the system $P(t)$.
2. Calculates the change of air volume $\Delta V_{\text{air}}(t)$ associated with the change in pressure $P(t)$ using look-up tables that correlate volume change associated with pressure change.
3. Compare the actual pressure $P(t)$ to a predetermined reference pressure and send appropriate signals to the stepper motor in the following manner:
 - If the actual pressure $P(t)$ is less than the reference pressure, a command signal is sent to the stepper motor to advance the piston.

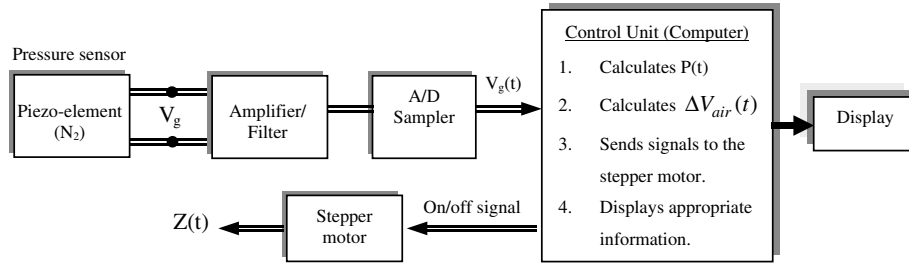


Fig. 2. Real-time closed loop pressure control.

- If the actual pressure $P(t)$ is greater than the reference pressure, a command signal is sent to the stepper motor to stop the piston.

4. Finite element analysis of the dispensing system

ANSYS [18] was used to model and analyze the system. This section provides detailed information on the simulations that were performed in order to assess the performance of the system and define optimal operating parameters. ANSYS also provided the capability to animate and visualize the ejection process of the droplets. During the simulation process, some variables involved in the dispensing process were varied in order to examine their effect on droplets generation. The characteristics that will be assessed include: (i) achieved droplet volume, (ii) verification on the occurrence of satellite droplets, (iii) achieved droplet ejection velocity, (iv) total pressure distribution inside the dispensing system, and (v) velocity distribution inside and outside the dispensing system. Finally, another important result that was made possible by ANSYS simulations is the ability to define actuation pressure tolerances towards the dispensing system's optimal operation.

This analysis is divided into three distinct steps: (i) building the model and meshing, (ii) applying loads and obtaining the solution, and (iii) reviewing the results. These are discussed in the following subsections.

4.1. Model development

The geometry and meshing of the model are depicted in Fig. 3 with the following relevant dimensions:

- Capillary inner diameter: 1 mm
- Nozzle diameter: 50 μm
- Capillary length: The required capillary length depends only on the total amount of liquid to be dispensed (liquid column length inside the capillary) which depends on the application. According to the simulations performed, variations in the liquid's column length had no effect on the dispensed liquid response. The liquid column length was 6 mm.

The properties of the liquid (water at 20°C) were taken as follows:

- Density: 998.2 kg/m^3
- Viscosity: 1.002e-3 N s/m^2
- Surface tension: 0.0728 N/m
- Static contact angle: 90°, kept as a constant value.

This structure displays geometric symmetry about a central axis and therefore is considered as an axisymmetric structure. Models of axisymmetric 3-D structures may be represented in equivalent 2-D form. After defining the model's geometry, each line in the geometry is assigned a

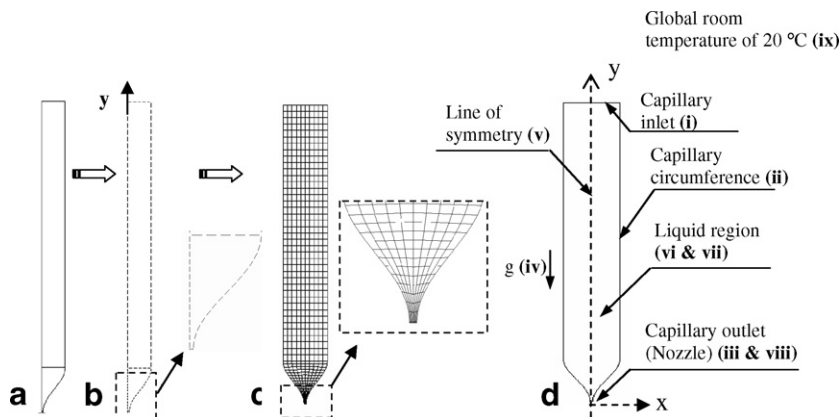


Fig. 3. Model geometry, finite element mesh and boundary conditions.

division pattern and number of divisions as depicted in Fig. 3(b). Assumptions were made about where the gradients are expected to be the highest (in this case the nozzle area), and the mesh was adjusted accordingly. If it is too coarse, the original mesh may not capture significant effects brought about through steep gradients in the solution. Conversely, elements may have very large aspect ratios with the long sides along directions with very low gradients. For the most accurate results, mapped meshing was used as it maintains a consistent mesh pattern along the boundary. A mapped area mesh that contains only quadrilateral-shaped elements was used in this case. As shown in Fig. 3(c), the finite element mesh in the converging area of the nozzle is much finer than the area above it. This mesh construction is extremely important not only for accurate results but also for a converging solution. It was very important to find an appropriate mesh pattern due to the geometry's high aspect ratio (ratio between length and diameter of the capillary) and the existence of a nozzle. Therefore, ANSYS Parametric Design Language (APDL) has been used to build the model in terms of parameters (variables). The mesh shape and size were optimized by running several simulations with different mesh sizes until an appropriate mesh was found. The mesh selection criteria were: (i) achieved solution convergence; (ii) required mesh resolution to capture the phenomenon accurately; and (iii) no noticeable changes in the solution were found as the mesh is made finer.

The boundary conditions are applied after the mesh is complete. The applied loads and boundary conditions are shown in Fig. 3(d) according to their numbering as follows:

- (i) Application of pressure pulses at the inlet of the capillary: The pressure applied at the capillary inlet is induced by the piston displacement and its form is depicted in Fig. 4. The pressure function was applied directly on the liquid column at the air–liquid interface; therefore, the air gap was not modeled in the FE model. The form of the signal emanating from the piezo-driven piston is similar to the signal shown in Fig. 4 that is driving the liquid. The two signals have basically the same form due to the fact that the air gap length is small so that wave propagation effects are negligible and as is shown in [19], a linear relationship (i.e., a second order transfer function) exists between the signal applied by the piezo-driven piston at the piston–air interface and the pressure pulse driving the liquid at the air–liquid interface.

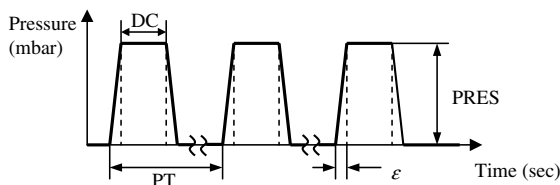


Fig. 4. Pressure function.

The linear relationship implies that the overall form of the piston signal is transferred to the liquid through the air column and no additional modes would appear [19]. In Fig. 4, DC denotes duty cycle, PT denotes period, PRES denotes the pressure amplitude and ε denotes the time needed for the function to rise or fall. In the performed analyses DC was varied between 1% and 10% and the effect of this variation is presented in Section 4.2. The period was taken to be 10 ms, which corresponds to an actuation frequency of 100 Hz. The pressure amplitude was varied between 200 mbar and 1200 mbar and the effect of this variation is also presented in Section 4.2. For an ideal pressure pulse, the value of ε should be zero. For the purpose of the simulations, this value could not be zero because it introduced very steep pressure gradients, which led to a diverging solution. A value of 100 ns was selected for ε .

- (ii) No slip conditions at the walls of the capillary. This boundary condition requires that velocities in the x - and y -directions at the capillary walls are zero – namely, $V_x = V_y = 0$.
- (iii) Zero gage pressure at the nozzle exit (liquid–air interface). Indicates atmospheric ambient pressure.
- (iv) Application of gravity loading.
- (v) Boundary condition for axisymmetric model. This boundary condition requires that the velocity in the x -direction (V_x) at the line of symmetry is zero.
- (vi) Defining the initial liquid region for VOF (volume of fluid) analysis [20].
- (vii) Apply VOF initial conditions.
- (viii) Apply surface tension effects.
- (ix) Global room temperature of 20 °C.

This is a transient problem of fluid system that involves fluid and non-fluid regions. The fluid is modeled as incompressible flow. The non-fluid region (air) outside the nozzle exit is also modeled and meshed in order to visualize the ejection process of the droplets. This area is recognized as the rectangular area placed right below the nozzle throughout Section 4.2.1. The conservation equations for viscous fluid flow and energy are solved in the fluid region, while only the energy equation is solved in the non-fluid region. For the FLOTRAN CFD elements, the velocities are obtained from the conservation of momentum principle, and the pressure is obtained from the conservation of mass principle. The temperature is obtained from the law of conservation of energy. A segregated sequential solver algorithm is used; that is, the matrix system derived from the finite element discretization of the governing equation for each degree of freedom is solved separately. The flow problem is non-linear and the governing equations are coupled. The sequential solution of all the governing equations, combined with the update of any temperature or pressure-dependent properties, constitute a global iteration. The number of global iterations required to achieve a converging solution may vary considerably, depending

on the size and stability of the problem. In the simulations, 25 global iterations were required in order to achieve a converging solution. Transport equations are solved for the mass fractions. The degrees of freedom are velocities, pressure, and temperature. In the solution, the following were incorporated: surface tension effects, volume of fluid (VOF) and Arbitrary Lagrangian–Eulerian (ALE) formulation for moving domains. In this problem, the fluid domain changes with time and the finite element mesh must move to satisfy the boundary conditions at the moving free surface of the droplets. Therefore, ALE formulation was used in order to solve this type of problem. The ALE formulation uses the displacement boundary conditions applied to update the finite element mesh. It determines the displacement at the beginning of each time step relative to the previous time step. For each time step, an elasticity based morphing algorithm updates the mesh. The algorithm ensures that boundary layers are retained (that is, nodes in a fine mesh area move less than nodes in a coarse mesh area). A transient analysis cannot proceed if morphing fails.

4.2. Analysis

4.2.1. Actuation pressure effects on the system's response

In the following analyses the pressure signal duty cycle is varied through the following values: 1%, 5% and 10%. The pressure amplitude is varied through the following values: 200, 350, 500, 900, and 1200 mbar. This *initial* range of pressures was found by trial and error by running several simulations to verify the response. Each duty cycle value is held constant while the pressure amplitude is varied between 200 and 1200 mbar. This provides 15 simulation runs. For each simulation run, $N = 500$ sample times were taken for a period of 5 ms, which provides a sampling frequency (SF) of 100 kHz. The purpose is to find the effects of the pressure amplitude and duty cycle variations on the following:

- Achieved droplet volume.
- Achieved droplet ejection velocity.
- Verification on the occurrence of satellite droplets.

The simulation results are summarized in Figs. 6–10. The collected data and the corresponding sampled frames are presented according to the scheme as depicted in Fig. 5. Few time samples (TS) were selected for presentation at the peak and few more time samples were also selected after the pulse. Each frame corresponds to a particular sample number (N), where the correlation between TS and N is given by $TS = (1/SF) \cdot N$. The sample number (N) at which each frame is shown is indicated under each frame.

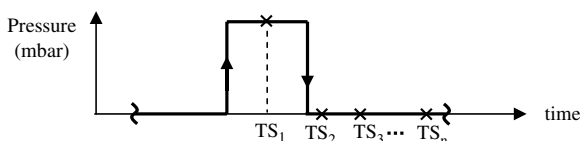


Fig. 5. Data collection scheme for volume fraction analysis (VOF).

A rectangular area placed right below the nozzle is defined as a void space where the evolution of droplets can be visualized. This expansion area begins right after the nozzle edge. This part of the simulations aims at investigating the evolution process of the droplets; therefore the area of interest (nozzle area and the area beneath it) is considerably magnified. The magnification scaling is kept consistent among frames that were taken within each simulation and sometimes among simulations.

The simulations begin with a pressure sweep with a duty cycle of 5% whereas it is anticipated that for longer pulse durations the amount of ejected liquid is larger. Doing so enables to run the simulations in a much lower resolution in terms of number of elements required for meshing the model. The number of elements that were used for a pressure sweep at DC of 5% was 5350, and the number of elements that were used for a pressure sweep at DC of 1% was 42,550 (including the non-fluid region). It was also found that using a coarse mesh for a pressure sweep at DC of 5% is good enough to properly capture the phenomenon. Using the same resolution for a pressure sweep at DC of 1% is not sufficient since the droplets cannot be seen due to their small size when compared to the size of each element in the mesh grid.

From the results of the simulation run for a pressure pulse with a duty cycle of 5% (pulse duration of 500 μ s) and pressure pulse amplitude of 200 mbar (Fig. 6(a)), it is quite apparent that this amount of pressure is not sufficient in order to eject a droplet. During the first 5 frames the droplet is hanging out of the nozzle. At the sixth frame however ($N = 86$), it can be seen that the droplet shrinks back into the capillary since there was not enough pressure to eject it. Since the applied pressure is removed, surface tension and viscous forces draw the liquid back to the capillary.

An excitation pressure of 350 mbar is sufficient enough in order to eject a droplet from the capillary nozzle as shown in Fig. 6(b). The first two frames ($N = 45$ and 71) were taken at the peak of the pulse and the rest were taken after the pulse at different consecutive times. At the third frame ($N = 86$) it can be seen that the drop stream is breaking off from the nozzle whereas the pressure is not applied anymore. As time passes, the detached drop stream takes a form of a sphere. The transformation process from a liquid stream to a spherical shape takes place due to internal viscous forces and surface tension effects. After the detachment at $N = 91$, a minuscule droplet that is hanging out at the tip of the nozzle is seen to be drawn back into the capillary as time passes. In this simulation set, it can be clearly seen that satellite droplets do not occur. The droplet's ejection velocity was found to be 2.73 m/s for $N = 71$. The droplet diameter at $N = 151$ was found to be 185 μ m which corresponds to a drop volume of 3.31 nL.

In another simulation set with a 5% duty cycle and 500 mbar actuation pressure it was found that the characteristics of the droplets ejection process were quite similar to the ones presented in Fig. 6(b). No satellite droplets were observed. The ejected droplet velocity (for $N = 71$) in this

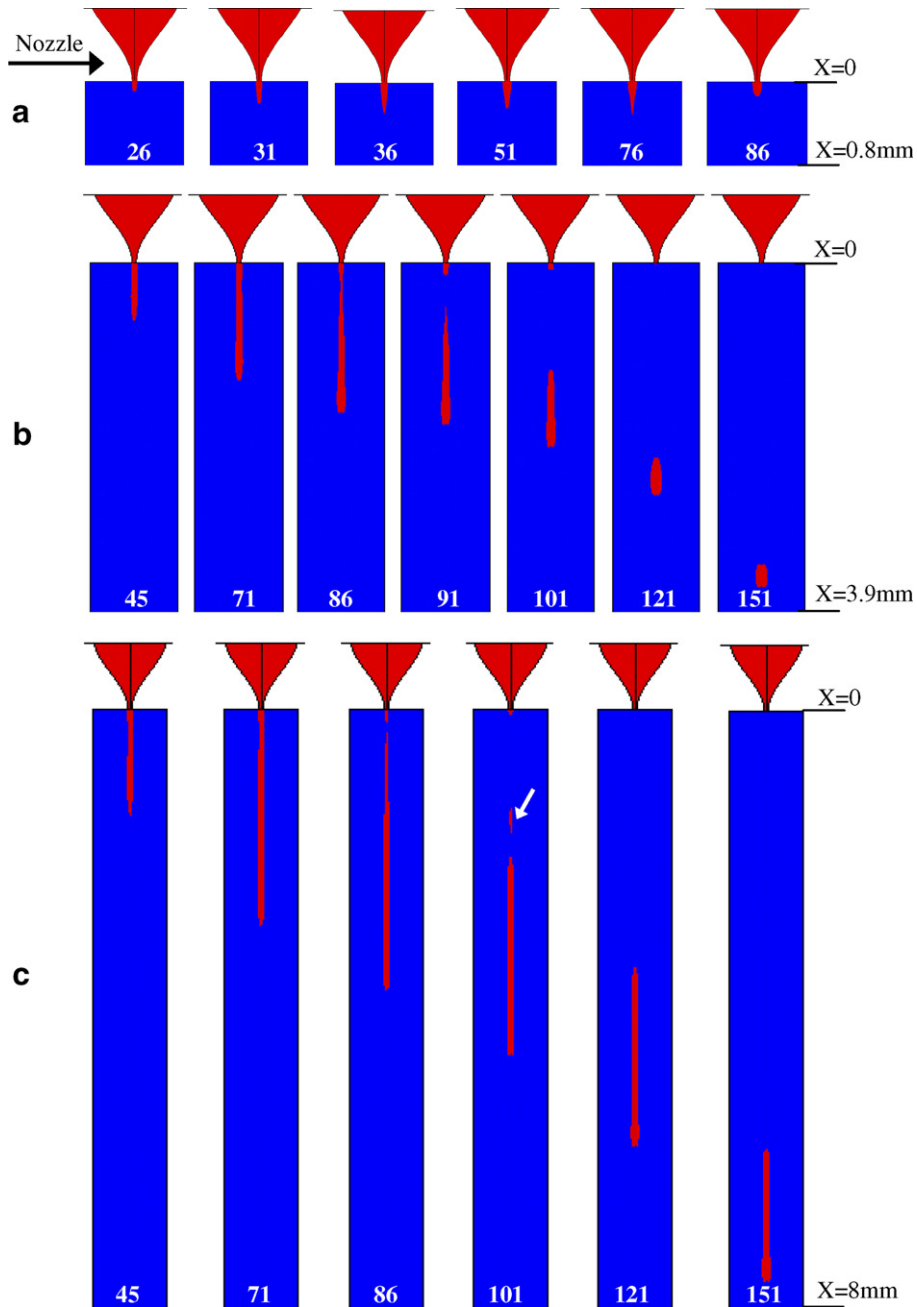


Fig. 6. Simulation results for duty cycle of 5% at: (a) 200 mbar; (b) 350 mbar; (c) 900 mbar.

case was found to be 4.23 m/s. The droplet diameter (at $N = 181$) was found to be 255 μm which corresponds to a drop volume of approximately 8.7 nL. As expected, these values of velocity of ejection and droplet volume are larger than those evaluated for a lower actuation pressure of 350 mbar.

In the simulation set presented in Fig. 6(c), satellite droplets occur at $N = 101$. It is important to mention that this satellite drop is first seen as a line and then vanishes at $N = 121$ due to a coarse mesh grid. The ejected droplet velocity for $N = 71$ in this case was found to be 5.75 m/s. The droplet diameter at $N = 151$ cannot be evaluated since at that position the liquid stream did not form a sphere yet. Clearly these values of velocity of ejection and droplet vol-

ume are larger than those evaluated for a lower pressure of 500 mbar. This value of pressure is too high since a drop having a shape of a sphere is formed too far from the nozzle exit (beyond 8 mm). In the application of Microarray spotting, the deposition of such a droplet would result in splashing on the substrate, which is undesired. For 1200 mbar actuation pressure the ejected liquid streams are longer with satellite droplets and droplet ejection velocity of 6.7 m/s.

Some general conclusions can be drawn based on the simulation runs at different pressures and at a duty cycle of 5%. First, it is clear that as the pressure increases, the ejected drop volume and velocity increase. Moreover, the

lengths of the ejected liquid streams are longer for higher pressures, which mean that a droplet with a shape of a sphere will be formed at a greater distance from the nozzle. Furthermore, satellite droplets were observed when the pressure was too high.

Based on simulation results for a pressure sweep with a duty cycle of 5%, the pressure range can be narrowed down to 350–500 mbar. This range ensures smaller drop volumes without satellite droplets. Based on this information and other results from previous simulations, only the results pertaining to 350 and 500 mbar will be presented from the simulations performed for a duty cycle of 1%. As was mentioned above, the number of mesh elements for a duty cycle of 1% is increased from 5350 to 42,550. The ejection phenomenon in this case is very precisely captured. Although not shown here, simulations pertaining to pressure actuations of 200, 900, and 1200 mbar were performed. For 200 mbar no ejection occurred and was similar to the results shown in Fig. 6(a). For actuation pressures of 900 and 1200 mbar, long liquid streams with satellite droplets were observed. The results pertaining to actuation pressure of 350 and 500 mbar are shown in Fig. 7(a) and (b), respectively.

It can be seen from Fig. 7(a) that an excitation pressure of 350 mbar is sufficient enough in order to eject a droplet from the capillary nozzle although the pulse duration is narrower (pulse duration of 100 μ s). In this simulation set, it can be seen that satellite droplets do not occur when the actuation pressure is 350 mbar, but they occur when the pressure is 500 mbar. In both cases, the ejected liquid streams are much shorter. This yields spherically formed droplets in a much less distance from the nozzle exit (less than 2 mm). This result is very important since it increases the throughput of the dispensing process in several applications where the time required for droplet deposition should be very short (e.g., Microarray fabrication).

The droplet ejection velocities were approximated and found to be 4.48 and 5.3 m/s for actuation pressures of

350 and 500 mbar, respectively. The droplet diameters were evaluated and were found to be 82 μ m and 99 μ m for actuation pressures of 350 and 500 mbar, respectively. These correspond to drop volumes of 288 pL and 508 pL.

In addition to the above, more simulation runs were performed with a pressure sweep at a duty cycle of 10%. The results were similar to those presented for a pressure sweep at a duty cycle of 5% except for much longer liquid streams. This result can be attributed to the fact that a larger duty cycle was used.

In summary, FEA analysis has shown that the input driving pressure parameters such as duty cycle and amplitude have significant effect on the system's response. These parameters have a direct effect on the occurrence of satellite droplets, on the ejected liquid volume and on the velocity of ejection. Large duty cycles mainly lead to droplets with larger volumes and vice versa. This makes sense since the longer the time, at which the pressure is applied, more liquid will be forced out of the nozzle. It was also shown that large actuation pressures produce satellite droplets. On the other hand, when the pressure was too low, it was not sufficient to expel a droplet from the nozzle. The simulation enabled to identify and quantify a useful pressure range for the dispensing system's operation and was found to be 350–500 mbar.

4.2.2. Velocity and pressure distributions

An investigation is presented next in order to find the distribution of the pressure and velocity gradients within the capillary as a function of time. Moreover, the velocity and pressure distributions of the droplet during the ejection process are investigated. The simulations in this part were performed using the best pressure signal parameters identified from the previous section – specifically, pressure amplitude of 350 mbar with a duty cycle of 1%. The collected data and the corresponding sampled frames are presented according to the scheme depicted in Fig. 8. The pulse begins at $N = 20$ (200 μ s). One time sample was taken just

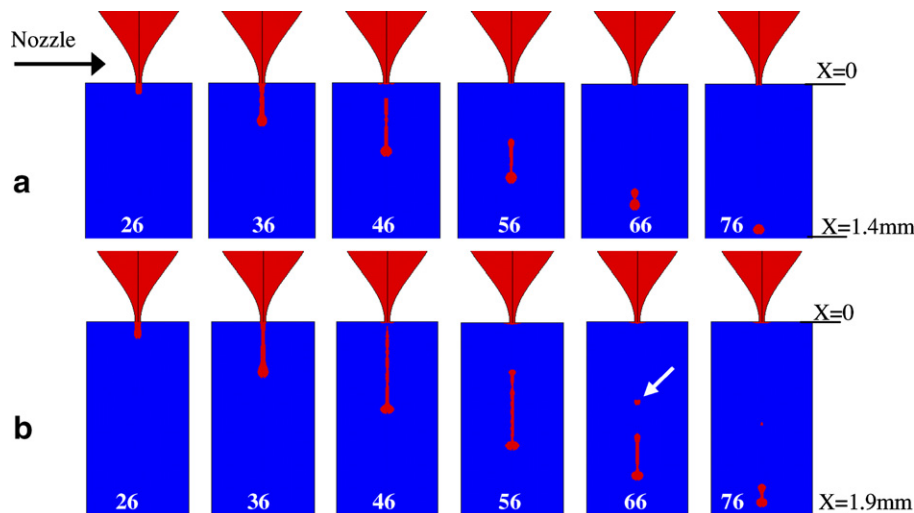


Fig. 7. Simulation results for duty cycle of 1% at: (a) 350 mbar; (b) 500 mbar.

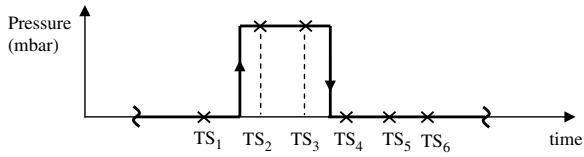


Fig. 8. Data collection scheme for pressure and velocity distributions.

before the rising edge of the pulse. Few time samples were taken at the peak and few more were taken after the pulse. The processed results of the data collected are presented in Figs. 9 and 10. Fig. 9 presents the velocity vector analysis at different time samples, while Fig. 10 depicts the pressure distribution analysis at different time samples.

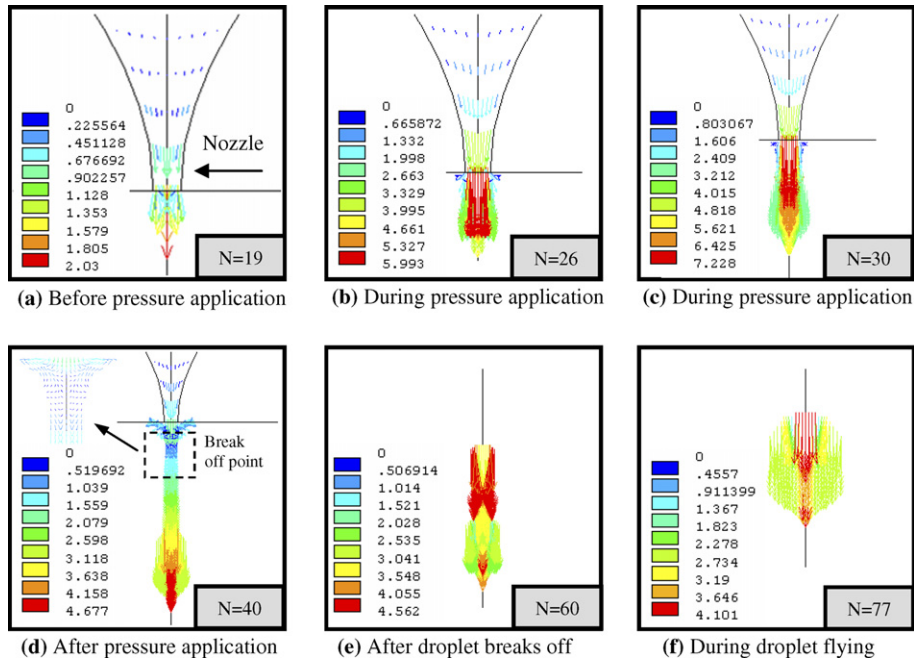


Fig. 9. Velocity vector analysis at different time samples.

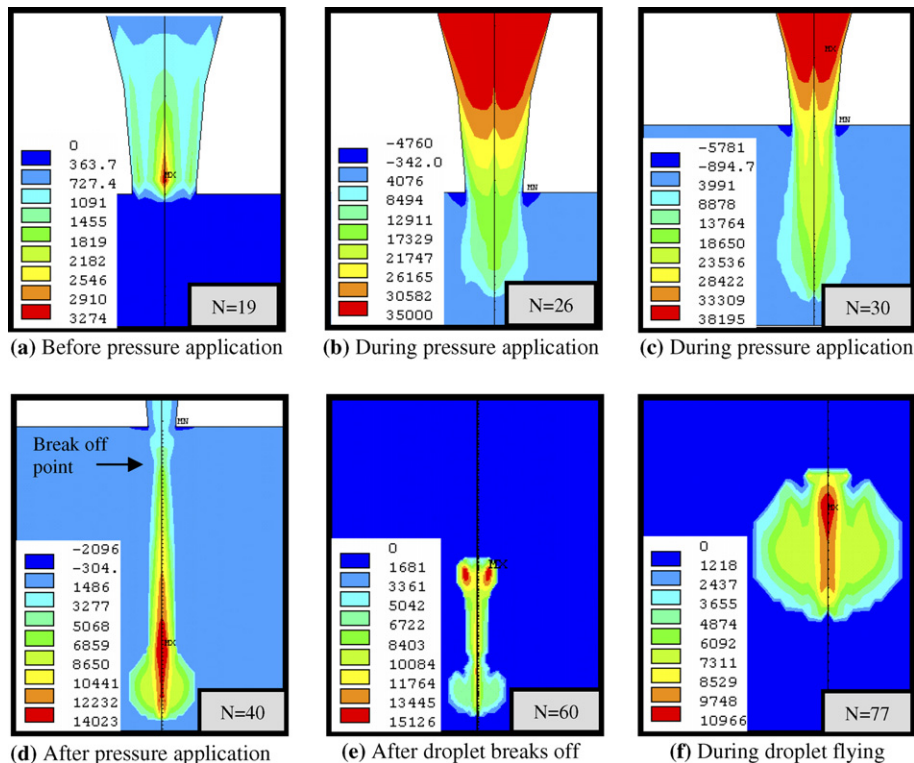


Fig. 10. Pressure distribution analysis at different time samples.

4.3. Conclusions

1. Figs. 9(a) and 10(a) depict the velocity and pressure distribution within the capillary just before the pressure pulse signal is applied. As expected, the velocity in the capillary at that time is zero. A magnification of the nozzle area shows that the velocity at the tip of the nozzle is not zero. This occurs due to localized oscillations of the liquid meniscus at the tip of the nozzle caused by a combination of surface tension forces and gravity. These oscillations could be observed when the volume of fraction (VOF) analysis was performed. Furthermore, the pressure within the capillary at the beginning exists only due to very minor hydrostatic pressure and due to local liquid oscillations at the lower open end where the liquid meniscus interacts with the ambient air. The effect of the hydrostatic pressure cannot even be seen since its effect is very small. The pressure gradient seen at the nozzle area is due to liquid meniscus oscillations that exert very small pressure waves at its surroundings.
2. Figs. 9(b) and 10(b) depict the velocity and pressure distribution within the capillary during the input pressure application. From these figures it can be seen that the velocity in the capillary is very low whereas the velocity at the nozzle area is significantly increased and is much higher than the velocity of the liquid on top of the nozzle area. The pressure distribution in the capillary, after an input pressure of 350 mbar is applied, is instantly changing from a very low value to an equally distributed pressure of 350 mbar that is equal to the value of the input pressure. A magnified view at the nozzle area reveals that the pressure at the nozzle exit is lower than the pressure above it. The existence of a descending pressure distribution at the nozzle area (as shown in Fig. 10(b)) enables the ejection of liquid from the nozzle.
3. Figs. 9(c) and 10(c) depict another time sample of velocity and pressure distribution within the capillary during the input pressure application. It can be seen from these figures that the pressure and velocity distributions are increased while the input pressure is still being applied. Furthermore, it can be seen from the velocity distribution plot that the highest velocity occurs at the core of the droplet. This indicates that the formed liquid jet is still in its inflation process before it breaks off.
4. Figs. 9(d) and 10(d) depict the velocity and pressure distribution within the capillary and outside the capillary after the input pressure is removed. The figures show that the pressure inside the capillary is dramatically decreased as expected. In this case, the liquid jet break off is captured in order to see what happens in terms of velocity and pressure distribution at that point. Fig. 9(d) shows that at the point of break off, the upper part of the liquid jet is pulling up (arrows are pointing up) while the lower part of the liquid stream is pulling down (arrows are pointing down). At the point of break off, the vertical component of the velocity is instantaneously zero (arrows are pointing to the left and right).

neously zero (arrows are pointing to the left and right). It can also be seen that the velocity distribution, from the tail at the point of break off to the head of the droplet, is increasing since the head is pulling down trying to be released from the tail. The pressure at the point of break off is decreased.

5. Figs. 9(e) and 10(e) depict the velocity and pressure distribution within the capillary and velocity and pressure distribution of the droplet after it breaks off from the nozzle. The pressure and velocity distributions in the capillary exhibit the same levels as it was before the pressure was applied. Fig. 9(e) shows that the velocity distribution, from the tail to the head of the droplet, is decreasing. This means that the tail has a greater velocity than that of the head since the tail is trying to catch up with the main drop and to become one spherical drop as shown in Fig. 10(f). This phenomenon can be attributed to the existence of internal viscous forces and surface tension forces.
6. Figs. 9(f) and 10(f) depict the velocity and pressure distribution of the droplet while flying. It now can be seen that the droplet has a spherical shape. This is reiterated by the fact that the pressure distribution at the top of the droplet is greater than the bottom indicating that the tail has compressed from an elongated form into a more spherical form.

5. Summary and conclusions

Dispensing systems for droplets generation are one of the important fluid handling devices in precise liquid dispensing and control. Categorization of droplet generators, in terms of dispensing modes and liquid transfer modes, were discussed in Section 2. Various actuation technologies for droplets generation, including piezoelectric, thermal-bubble, pneumatic, thermal buckling, focused acoustic wave, electrostatic, and inertial actuation, have been employed in generation of droplets in the range of microliters to picoliters. Compared to other methods, piezoelectric droplet generators have the advantage of high frequency response, controllable droplet size, and the potential to eliminate satellite drops. Thermal-bubble based actuation is characterized by larger actuation deformation and simpler design, but has the drawback of being temperature and liquid properties dependent. Piezoelectric demand mode does not create thermal stress on the fluid, which decreases the life of both the device and fluid. Furthermore, it does not depend on the thermal properties of the fluid to impart acoustic energy to the working fluid.

In Section 3, a design of a dispensing system for droplets generation was presented. All the stages in the dispensing process and the initialization process were discussed. It was shown that the proposed design of a dispensing system potentially overcomes various problems of existing systems and adds a great deal of functionality to the dispensing process.

In Section 4, ANSYS finite element modeling of the system was pursued. ANSYS was used to animate and visualize the operation of the device. The droplet's generation and evolution process, after it leaves the nozzle, were also achieved. Finally, ANSYS simulations were used to define actuation pressure tolerances towards the dispensing system's desired response.

Acknowledgement

This work was partially supported by Manufacturing and Materials Ontario (MMO) and Engineering Services Inc. (ESI).

References

- [1] Nielsen NJ. History of thinkjet printhead development. *Hewlett-Packard J* 1985;36(5):4–10.
- [2] Sweet RG. High frequency recording with electrostatically deflected ink-jets. *Rev Sci Instrum* 1965;36:131.
- [3] Ulmke H, Wriedt T, Bauckhage K. Piezoelectric droplet generator for the calibration of particle-sizing instruments. *Chem Eng Technol* 2001;24:265–8.
- [4] Cooley P, Wallace D, Antohe B. application of ink-jet printing technology to BioMEMS and Microfluidic Systems. In: *Proceedings, SPIE conference on microfluidics and BioMEMS*, October 2001.
- [5] Switzer GL. A versatile system for stable generation of uniform droplets. *Rev Sci Instrum* 1991;62:2765–71.
- [6] Le HP. Progress and trends in ink-jet printing technology. *J Imaging Sci Technol* 1998;42(1):49–62.
- [7] Tseng FG. A micro droplet injector system, Ph.D. Dissertation. University of California, Los Angeles; 1998.
- [8] Bogy DB, Talke FE. Experimental and theoretical study of wave propagation in drop-on-demand ink-jet devices. *IBM J Res Dev* 1984;29:314–21.
- [9] Aden JS, Bohorquez JH, Collins DM, Crook MD, Garcia A, Hess UE. The third generation HP thermal ink-jet printhead. *Hewlett-Packard J* 1994;45:41–5.
- [10] Wallace DB. A method of characteristics model of a drop-on-demand ink-jet device using an integral method drop formation model', ASME publication 89-WA/FE-4; 1989.
- [11] Rayleigh JWS. On the instability of jets. *Proc London Math Soc* 1879;10(4):4–13.
- [12] Tisone TC. Dispensing Systems for Miniaturized Diagnostics. *IVD Tech Mag* 1998(May).
- [13] <http://las.perkinelmer.com>.
- [14] <http://www.incyte.com>.
- [15] Rose D. Microfluidic technologies and instrumentation for printing DNA microarrays, Cartesian Technologies Inc., California, Chapter 2.
- [16] Jones SE et al. Piezoelectric materials and their applications. *Advanced ceramic materials, key engineering materials*, vols. 122–124. Switzerland: Trans Tech Publications; 1996. p. 451–462, © 1996.
- [17] Morgan Electroceramics Technical Publications: www.morgan-electroceramics.com/techpub1.html.
- [18] www.ansys.com.
- [19] Evensen HT, Meldrum DR, Cunningham DL. Automated fluid mixing in glass capillaries. *Rev Sci Instrum* 1998;69(2):519–26.
- [20] ANSYS, Inc. Theory Reference, subsection 7.3: Volume of fluid method for free surface flows, Available from: http://www.oulu.fi/atkk/tkpalv/unix/ansys-6.1/content/theory_toc.html.